IEEE Access
Multidisciplinary | Rapid Review | Open Access Journal

Received January 16, 2019, accepted February 1, 2019, date of publication February 5, 2019, date of current version March 25, 2019.

Digital Object Identifier 10.1109/ACCESS.2019.2897572

Prediction of Load-Carrying Capacity in the Radial Direction for Piezoelectric-Driven Ultrasonic Bearings

HE LI[1], (Member, IEEE), AND ZONGQUAN DENG[2]
[1]College of Mechanical and Electronic Engineering, Shandong University of Science and Technology, Qingdao 266590, China
[2]State Key Laboratory of Robotics and System, Harbin Institute of Technology, Harbin 150001, China

Corresponding author: He Li (lihe_hit@163.com)

This work was supported in part by the Program of Introducing Talents of Discipline to Universities under Grant B07018, and in part by the Fundamental Research Funds for the Central Universities under Grant HIT.NSRIF.2014051.

ABSTRACT This paper presents a theoretical modeling method on radial levitation force for ultrasonic bearings actuated by piezoelectric transducers with the aim of predicting their load-carrying capacity. The finite difference method is adapted to calculate the model, which is represented by a high-order multidimensional partial differential equation. The static levitation force testing experiments validate that the established mechanical model can interpret the experimental data well. This model also reveals that the ultrasonic bearing's levitation mechanism under the comprehensive action of near-field acoustic levitation effect and hydrodynamic effect when the bearing operates at high speeds. Some key factors including bearing's dynamic parameters, working media, clearance sizes, and environmental conditions that influence the ultrasonic bearing's levitation effect are discussed. The analysis of these factors can guide the ultrasonic bearing's structural design and the selection of the ultrasonic bearing's working parameters.

INDEX TERMS Ultrasonic bearings, piezoelectric drive, levitation force, Reynolds equation, finite difference method.

I. INTRODUCTION

The basic manufacturing technology and key parts are the cornerstones of the development of the equipment manufacturing industry. They determine the performance, quality and reliability of the major equipments and devices. A bearing is a kind of distinctly important basic component of a machine. The design and development of novel bearings based on basic frontier technology will contribute to the transformation, upgrading and sustainable development of high-end intelligent equipments [1]–[3].

As a kind of promising non-contact bearings, ultrasonic bearings actuated by smart materials such as PZT ceramics show a good application prospect in high-speed machines and precision-measuring devices [4], [5]. Compared with the conventional non-contact bearings such as hydrostatic bearings, hydrodynamic bearings and electromagnetic suspending bearings, the ultrasonic bearings are environmentally friendly bearings using air as working medium. They have no noise pollution and need low maintenance cost. Since the bearing's service life is determined by the longevity of the smart materials, the bearing's service life can be extended if the material property is improved [6], [7]. On account of that the ultrasonic bearing's operation is based on the near-field acoustic effect and hydrodynamic lubrication effect, this type of bearings shows extremely low friction torque and high limit speed. In addition, the controlling method of the ultrasonic bearing is simple and flexible, due to the approximate linear relation between the input voltage and the output vibration amplitude [8], [9].

The levitation force is a vital parameter representing the bearing's load-carrying capacity. The accurate prediction of levitation force will contribute to the bearing's design and optimization, and the establishment of the levitation model will enhance the comprehension to levitation process and levitation mechanism. More importantly, some effective measures to improve the bearing's levitation force can be found, which will be beneficial to broaden the bearing's application fields. Generally, the research of the ultrasonic bearing is mainly derived from two different points of view: one is

The associate editor coordinating the review of this manuscript and approving it for publication was Chao Tan.

the non-linear acoustics, the other one is the fluid dynamics. Nomura firstly conducted the research on the acoustic field excited by longitudinal vibration based on fluid dynamics method [10]. A gas dynamic equation was established, and MacCormack finite difference scheme was adopted to solve the equation. This model can predict the levitation force generated by longitudinal vibration for a levitation system with specified size and shape. Liu *et al.* [11] and Li *et al.* [12] studied the acoustic field excited by flexural vibration of a metal disk and investigated the suspending force generated by the flexural vibration. Considering the vibrator surface should be nonuniform, a theoretical procedure was derived by using real measured surface displacement distributions as boundary conditions to solve the squeeze gas film problem. Li *et al.* [13] also analyzed the gas inertia and boundary effect's impacts on the suspending force to improve the model. With regard to acoustic field excited by flexural vibration, Hu *et al.* [14] carried out a research on the suspending stability and interpreted the generated reason of horizontal restoring force on suspended object based on an equivalent block-spring model. It was found that the property of the fluid between the levitated disk and the vibrator has a large effect on the stability. The theoretical results showed that increasing the weight per unit area of the levitated object increases the stability for a given vibrator velocity. In terms of ultrasonic journal bearings, a majority of suspending theories for rotor are derived from the levitation theories for flat object. The reason is that if the ultrasonic journal bearing's vibration surface is spread out in the circumferential direction, the suspension problem to rotor is transformed into the suspension to flat object. Zhao et al. investigated squeeze film type ultrasonic levitation theoretically to improve the achievable levitation capacity. Excursion ratio and squeeze number were found to be the most crucial parameters that determine the levitation capacity. A good surface finishing and form accuracy are also important for a squeeze film levitation system to achieve higher levitation capacity [15], [16]. Stolarski *et al.* [17], [19] and Stolarski [18] established a modified three-dimensional Reynolds equation for an aerodynamic bearing to investigate its suspended rotor's trajectory changing rule under the perturbation and validated the suspending force's influence on the bearing's running stability. For bearings with complex structures such as ball-shaped bearing used in the gyroscope, the finite element softwares (ANSYS or COMSOL) are generally used to study the ultrasonic bearing's levitation characteristics [20].

For ultrasonic bearings actuated by several transducers, the bearings operate based on combined suspending action of the near-field acoustic levitation effect and hydrodynamic effect. The thickness of the bearing's air film is time-varying which is different from traditional air bearings, and the influences from boundary effect, gas inertia and rarefaction effect for ultra-thin air film become remarkable to the bearing's load-carrying capacity. Moreover, the hydrodynamic effect will play an important role in levitation process when the rotor in eccentric state runs at a high speed. To really reflect the bearing's working condition, a levitation force model based on modified Reynolds equation is built which is described as a type of multidimensional high-order partial differential equation. The Crank-Nicolson weighted implicit difference scheme is adopted to solve the levitation force model. A levitation force testing method is also proposed to validate the theoretical results. The influences of bearing's kinetic parameters, bearing clearance, working medium, ambient temperature and relative humidity on the levitation force are analyzed for the sake of finding some measures to improve the bearing's load-carry capacity.

II. ULTRASONIC BEARING ACTUATED BY PIEZOELECTRIC TRANSDUCERS

A. STRUCTURE OF ULTRASONIC BEARING

The excitation sources of ultrasonic bearings can be divided into two types: magnetostrictive transducers and piezoelectric transducers. Piezoelectric transducers are commonly used in the development of ultrasonic bearings due to their lower cost and higher performance. There are also two types of piezoelectric transducers: the surface mount type and the sandwich type. Compared with surface mount type piezoelectric transducers, the sandwich type piezoelectric transducers have more excellent output characteristics and longer service life. Thus, a majority of the ultrasonic bearings proposed by researchers are based on sandwich type piezoelectric transducers. As shown in Fig. 1, according to the number of transducers used in the bearing, ultrasonic bearings can be divided into single-axis levitating bearing, double-axis levitating bearing, three-axis levitating bearing and four-axis levitating bearing, etc. The envelop angle to a rotor is generally less than 180° for the ultrasonic bearing driven by single piezoelectric transducer. In this case, the bearing can not envelop the rotor in the whole circumferencial direction. In order to realizing the stable suspension to the rotor running at high speeds, several transducers are needed to design and develop the ultrasonic bearing.

With the increase of the levitating axis number or the transducer number, the structure of the bearing becomes more complicated, and the development cost and controlling difficulty will raise. Meanwhile, in order to ensure the uniformity of the vibration amplitude on bearing's radial radiation surface, the envelop angle of the each transducer should not be too large. Given the above all, the three-axis levitating bearing is a relative ideal ultrasonic bearing structure.

B. WORKING PRINCIPLE OF ULTRASONIC BEARING ACTUATED BY THREE TRANSDUCERS

In order to realize the stable suspension to the rotor, three piezoelectric transducers are used which are circumferentially equispaced in a housing, with their center lines going through the rotation center of the rotor. The structural representation of the bearing is shown in Fig. 2. Each transducer has a concave surface on the radiator, and the envelop angle of each transducer is about 117°. The design and manufacturing

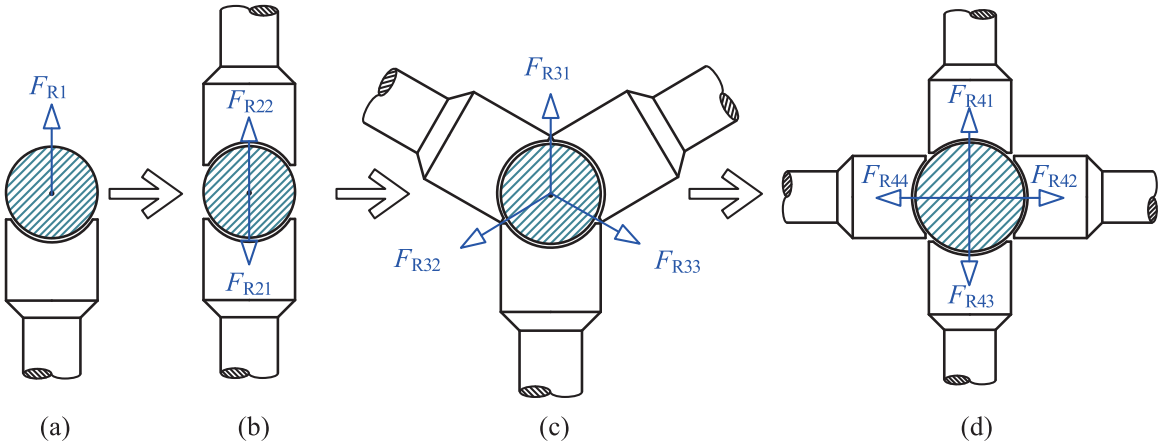

FIGURE 1. Schematic diagram of multi-axis levitating bearing. (a) Single-axis. (b) Double-axis. (c) Three-axis. (d) Four-axis.

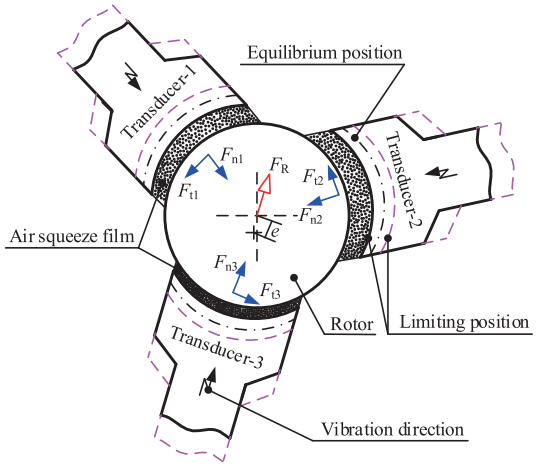

FIGURE 2. Working principle of ultrasonic bearing actuated by three piezoelectric transducers. (a) Structure of three-axis levitating bearing. (b) Self-aligning working principle.

technique parameters of the three transducers are completely consistent in order to obtain the same output characteristics under identical excitation voltage. In this article, an ultrasonic bearing motivated by three piezoelectric transducers is studied, and the same research method can be generalized to ultrasonic bearings excited by four or more piezoelectric transducers. The suspension forces generated by the three transducers form the three-point support. Due to the negative correlation between the suspending force and the thickness of the air film, the smaller the bearing gap, the higher the levitation force. Therefore, when the axis of the rotor O_1 deviates from the center O of the bearing, the levitation force F_{R3} will become large. Conversely, the levitation force F_{R12} will become small. Eventually, a resultant force F_R pointing to the center of the bearing will be generated. Thus,the bearingąŕs levitation force will automatically keep the rotor at an equilibrium position.

III. LEVITATION FORCE MODEL BASED ON MODIFIED REYNOLDS EQUATION

A. HYDRODYNAMIC EQUATION BASED ON REYNOLDS EQUATION

Reynolds equation proposed by Osborne Reynolds in 1886 deals with the pressure distribution in fluid film between two opposing surfaces in relative motion [21]. Firstly, the following assumptions are made:

(a) The fluid is Newtonian fluid, and the fluid state is laminar flow;

(b) No external force is applied on the fluid, and inertia force and body force are ignored;

(c) Pressure change and velocity component in the thickness direction are neglected due to that the air film's thickness is very small.

The two-dimensional fluid's dynamic equation is acquired in the rectangular coordinate system shown in Fig. 3(a). The expression of the equation is

$$\frac{\partial}{\partial x}(ph^3\frac{\partial p}{\partial x})+\frac{\partial}{\partial y}(ph^3\frac{\partial p}{\partial y}) = 6\mu(u_1+u_2)\frac{\partial(ph)}{\partial x}+6\mu(v_1+v_2)\frac{\partial(ph)}{\partial y}+12\mu\frac{\partial ph}{\partial t} \quad (1)$$

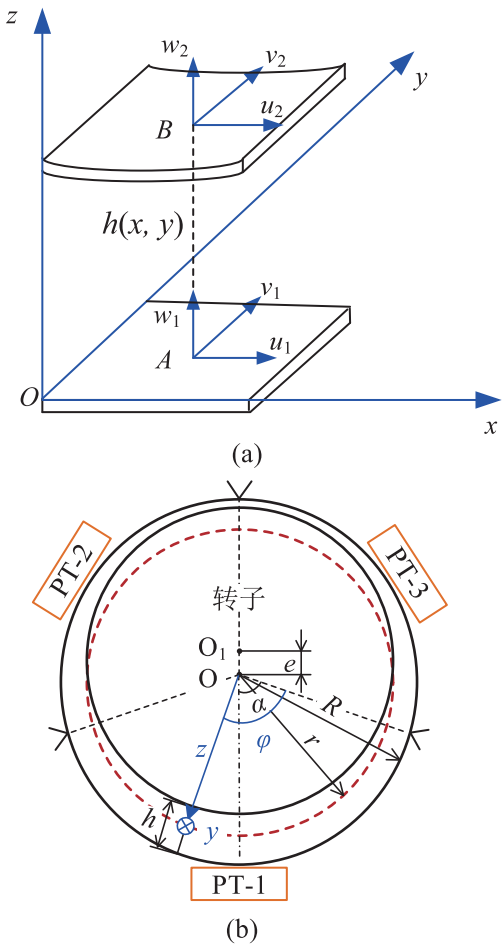

FIGURE 3. Coordinate systems used in the hydrodynamic models of fluid film between two plates with relative motion and bearing's air film. (a) Rectangular coordinate system. (b) Cylindrical coordinate system.

where p, μ, and h are the air film's pressure, dynamic viscosity, air film's thickness; u_1, u_2, v_1, and v_2 represent the lower and upper plate's velocities in the x and y directions respectively.

If the air only flows in the x direction, the equation above will be

$$\frac{\partial}{\partial x}(ph^3\frac{\partial p}{\partial x})+\frac{\partial}{\partial y}(ph^3\frac{\partial p}{\partial y})=6\mu(u_1+u_2)\frac{\partial(ph)}{\partial x}+12\mu\frac{\partial ph}{\partial t} \tag{2}$$

If the fluid dynamic equation is transformed from the rectangular coordinate system shown in Fig. 3(a) into the cylindrical-coordinate system shown in Fig. 3(b), we get

$$\frac{\partial}{\partial \varphi}(ph^3\frac{\partial p}{\partial \varphi})+\frac{\partial}{\partial y}(r^2ph^3\frac{\partial p}{\partial y})=6\mu r(u_1+u_2)\frac{\partial(ph)}{\partial \varphi}+12\mu r^2\frac{\partial ph}{\partial t} \tag{3}$$

According to the bearing's real operating state, the rotor runs at a high speed of n_0, and the bearing's inner ring does not move in the circumferential direction. That is $u_1 = 0$, and $u_2 = \frac{\pi \cdot r \cdot n_0}{30}$. The Eq.(3) is changed as

$$\frac{\partial}{\partial \varphi}(ph^3\frac{\partial p}{\partial \varphi})+\frac{\partial}{\partial y}(r^2ph^3\frac{\partial p}{\partial y})=6\mu r u_2\frac{\partial(ph)}{\partial \varphi}+12\mu r^2\frac{\partial ph}{\partial t} \tag{4}$$

In the Eq.(4), the expression of air film's thickness h is

$$h = c_r(1+\varepsilon\cos(\varphi))+a_0\cos(\omega t)=c_rH \tag{5}$$

where c_r, ε, φ, a_0, and ω present the radius gap, ratio between the eccentricity e and radius gap c_r, the position angle shown in Fig. 3(b), amplitude and angular frequency of the vibration on the bearing's inner ring, respectively. H is the non-dimensional air film thickness.

B. INERTIAL EFFECT

The dominant factors that affect the ultrasonic bearing's air squeeze-film's pressure are the gas's viscous force and inertia force. In hydrodynamic lubrication theory, the Reynolds number is introduced to represent the ratio of the viscous force and inertia force. In terms of the ultrasonic bearings, the Reynolds number Re can be modified as

$$Re = 2\pi\rho_0 h_0^2 f/\eta_0 \tag{6}$$

where f is the frequency of acoustic wave, h_0 is the vertical thickness of air film, and η_0 is the air's dynamic viscosity. Generally, $f \geq 16$ kHz, $h_0 \in (10, 100)$ μm, and $\eta_0 = 1.771 \times 10^{-5}$ Pa·s.

According to Eq.(6), the value of Re can be estimated. It is found that Re is on the verge of 1, or even greater than 1. In this case, the gas inertia force is dominant to levitation force compared with viscous force. Therefore, the influence of the air's inertia force should be taken into account in the levitation force modeling process. The levitation force model can be derived from the Navier-Stokes equation.

For a fluid element $\mathrm{d}V = \mathrm{d}x \times \mathrm{d}y \times \mathrm{d}z$ in the air gap between the bearing and the rotor shown in Fig. 4, the expression of Navier-Stokes equation is

$$\rho\frac{d\mathrm{V_{flow}}}{dt}=\rho\,\mathrm{F}-\nabla\cdot\mathrm{p}+\mu\nabla^2\mathrm{V_{flow}}+\frac{1}{3}\mu\nabla\,(\nabla\cdot\mathrm{V_{flow}}) \tag{7}$$

where V presents the flow velocity, and $V_{\mathrm{flow}} = (u, v, w)$. F and p are the body force and pressure in the air film respectively, and $F = (f_x, f_y, f_z)$, $p = (p_x, p_y, p_z)$. ∇ is the laplace operator.

It is assumed that the flow in the air film is laminar flow and the gas viscosity is constant. Since the order of the air squeeze film thickness is 10^{-5} m, which is three orders smaller than the dimensions of the bearing's vibrating surface (with order of 10^{-2} m), pressure gradient in the z direction $\frac{\partial p}{\partial z} \approx 0$. In the bearing's suspending process, there is no external force acted on the air film. Thus $f_x = f_y = f_z = 0$. The Navier-Stokes equation can be simplified as

$$\begin{cases}\rho\dfrac{du}{dt}=-\dfrac{\partial p}{\partial x}+\eta\dfrac{\partial^2 u}{\partial z^2}\\ \rho\dfrac{dv}{dt}=-\dfrac{\partial p}{\partial y}+\eta\dfrac{\partial^2 v}{\partial z^2}\end{cases} \tag{8}$$

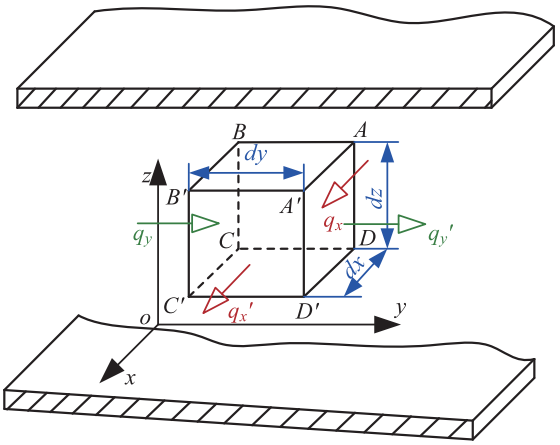

FIGURE 4. A fluid element in the air gap between the bearing and the rotor.

When the ultrasonic bearing is working, the rotor runs at a high speed, but the bearing's inner ring keeps static relative to rotor in the circumferential direction. According to the velocity boundary conditions: $u(0) = 0$, $u(h) = u_2$; $v(0) = v(h) = 0$, the Eq.(8) is changed as

$$\begin{cases} u = -\dfrac{1}{2\eta}\dfrac{\partial p}{\partial x}z(h-z) + \dfrac{u_2}{h}z \\ v = -\dfrac{1}{2\eta}\dfrac{\partial p}{\partial y}z(h-z) \end{cases} \tag{9}$$

Based on the law of conservation of mass, that is, for any one micro fluid unit shown in Fig. 4 in air film, incremental mass of air in the micro-unit is equal to the mass of air flowing into the micro-unit within the same time, we get

$$\frac{\partial(\rho q_x)}{\partial x} + \frac{\partial(\rho q_y)}{\partial y} = \frac{\partial(\rho h)}{\partial t} \tag{10}$$

According to the state equation of the compressible gas which can be expressed as

$$\frac{p}{p_0} = \frac{\rho}{\rho_0} \tag{11}$$

We combine these equations above and obtain the following hydrodynamic equation

$$\begin{aligned} &\frac{\partial}{\partial x}\left[\frac{ph^3}{12\eta}\left(1 - \frac{\rho_0}{p_0}\frac{ph}{4\eta}\frac{\partial h}{\partial t}\right)\frac{\partial p}{\partial x} + \frac{\rho_0}{p_0}\frac{p^2u_2h^2}{24\eta}\frac{\partial h}{\partial t}\right] \\ &\quad + \frac{\partial}{\partial y}\left[\frac{ph^3}{12\eta}\left(1 - \frac{\rho_0}{p_0}\frac{ph}{4\eta}\frac{\partial h}{\partial t}\right)\frac{\partial p}{\partial y}\right] \\ &= \frac{u_2}{2}\frac{\partial ph}{\partial x} + \frac{\partial(ph)}{\partial t} \end{aligned} \tag{12}$$

If the transformation of coordinates shown in Fig. 3 is used in the above Eq.(12), the ultrasonic bearing's hydrodynamic equation expression is obtained which is listed as follows

$$\begin{aligned} &\frac{\partial}{r\partial\varphi}\left[\frac{ph^3}{12\eta}\left(1 - \frac{\rho_0}{p_0}\frac{ph}{4\eta}\frac{\partial h}{\partial t}\right)\frac{\partial p}{r\partial\varphi} + \frac{\rho_0}{p_0}\frac{p^2u_2h^2}{24\eta}\frac{\partial h}{\partial t}\right] \\ &\quad + \frac{\partial}{\partial y}\left[\frac{ph^3}{12\eta}\left(1 - \frac{\rho_0}{p_0}\frac{ph}{4\eta}\frac{\partial h}{\partial t}\right)\frac{\partial p}{\partial y}\right] \\ &= \frac{u_2}{2}\frac{\partial ph}{r\partial\varphi} + \frac{\partial(ph)}{\partial t} \end{aligned} \tag{13}$$

C. RAREFACTION EFFECT AND SURFACE TOPOGRAPHY EFFECT

The thickness of the air film between the bearing and the rotor is in a micron order. This film can be regard as a ultra-thin gas film. For ultra-thin gas film, the influence of the gas molecule's discrete features and surface microtopography on the bearing's levitation force is remarkable. Therefore, the rarefaction effect and surface topography effect should be taken into account in the modeling process.

Based on Pandey and Pratap's studies [22], [23], pressure flow factors are introduced which are expressed as

$$\begin{cases} k_\varphi = 1 + g\dfrac{\sigma_1^2 + \sigma_2^2}{h^2}\left(1 - \dfrac{f^2}{g}\dfrac{1}{\lambda+1}\right) \\ k_y = 1 + g\dfrac{\sigma_1^2 + \sigma_2^2}{h^2}\left(1 - \dfrac{f^2}{g}\dfrac{\lambda}{\lambda+1}\right) \end{cases} \tag{14}$$

where σ_1 and σ_2 are root mean squared values indicating the degree of the profile's deviation from the average within a sampling length of journal surface and bearing radiation surface. λ is Peklenik number which is defined to describe the degree of non-isotropy of a rough surface. If $\lambda = 1$, the profile topography is isotropic. $\lambda < 1$ means that the three-dimensional topography is transverse roughness, in other words, interacting surfaces of the bearing have the topography of long narrow ridges and valleys running in the direction against the air flow, while $\lambda > 1$ means that the three-dimensional topography is longitudinal roughness. The value of the λ is generally related to the processing method and can be measured by an atomic force microscope. f and g are functions related to gas rarefaction effect, which can be expressed as

$$\begin{cases} f = 3 + \dfrac{6bcD^c - 3a\sqrt{\pi}/D}{Q(D)} \\ g = 3 + \dfrac{3bc(c+5)D^c - 6a\sqrt{\pi}/D}{Q(D)} \end{cases} \tag{15}$$

where a, b and c are three adjustment coefficients, D is inverse Knudsen number, and $Q(D)$ is the non-dimensional pressure flow factor representing the rarefaction effect. If the rarefaction effect is neglected, then $f = g = 3$.

If the bearing's Eq.(13) is modified using the Eq.(14), we get

$$\begin{aligned} &\frac{\partial}{r\partial\varphi}\left[k_\varphi\frac{ph^3}{12\eta}\left(1 - \frac{\rho_0}{p_0}\frac{ph}{4\eta}\frac{\partial h}{\partial t}\right)\frac{\partial p}{r\partial\varphi} + k_\varphi\frac{\rho_0}{p_0}\frac{p^2u_2h^2}{24\eta}\frac{\partial h}{\partial t}\right] \\ &\quad + \frac{\partial}{\partial y}\left[k_y\frac{ph^3}{12\eta}\left(1 - \frac{\rho_0}{p_0}\frac{ph}{4\eta}\frac{\partial h}{\partial t}\right)\frac{\partial p}{\partial y}\right] \\ &= k_\varphi\frac{u_2}{2}\frac{\partial(ph)}{r\partial\varphi} + \frac{\partial(ph)}{\partial t} \end{aligned} \tag{16}$$

The variables in above equation is dealt with dimensionless method, and the following dimensionless parameters are defined: $\phi = \frac{\varphi}{2\pi}$, $(0 \le \phi \le 1)$; $Y = \frac{y}{L/2}$, $(-1 \le Y \le 1)$; $P = \frac{p}{p_o}$; $H = \frac{h}{c}$; $T = t$; $U = u_2$.

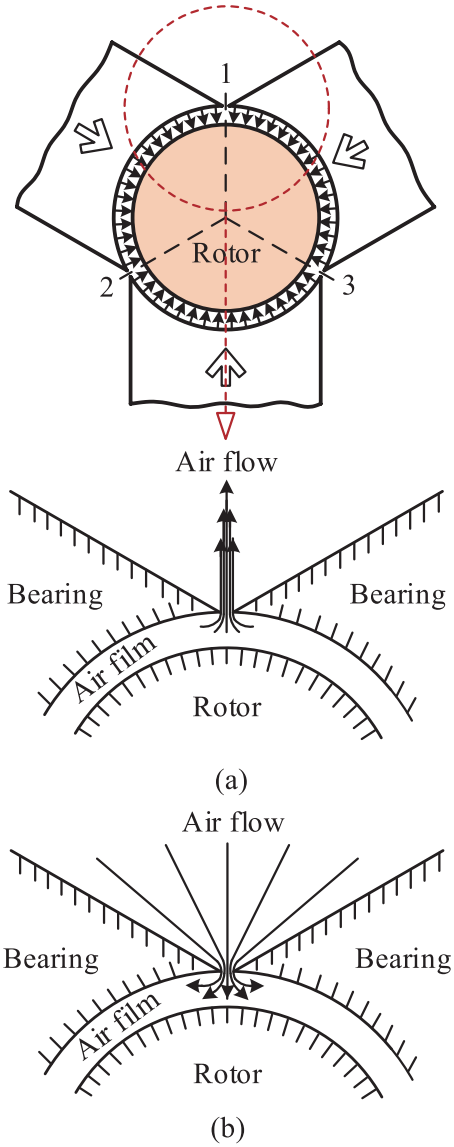

FIGURE 5. Schematic diagram of boundary effect in air film. (a) The positive squeeze stage. (b) The positive squeeze stage.

The bearing's non-dimensional hydrodynamic equation considering air inertia, rarefaction effect and surface topography is acquired.

$$\begin{aligned}&\frac{\partial}{\partial\phi}\left[k_\varphi\left(1-\rho_0c^2\frac{PH}{4\eta}\frac{\partial H}{\partial T}\right)PH^3\frac{\partial P}{\partial\phi}\right]\\&\quad+\frac{\partial}{\partial\phi}\left[k_\varphi\frac{2\pi^2r^2\rho_0U}{p_0}P^2H^2\frac{\partial H}{\partial T}\right]\\&\quad+\frac{16\pi^2r^2}{L^2}\frac{\partial}{\partial Y}\left[k_y\left(1-\rho_0c^2\frac{PH}{4\eta}\frac{\partial H}{\partial T}\right)\frac{\partial P}{\partial Y}PH^3\right]\\&=k_\varphi\frac{12\pi r\eta U}{p_0c^2}\frac{\partial(PH)}{\partial\phi}+\frac{48\pi^2r^2\eta}{p_0c^2}\frac{\partial(PH)}{\partial T}\end{aligned}\tag{17}$$

D. BOUNDARY EFFECT

The pressure in the gap between the bearing and the rotor equals to ambient pressure if the air's inertia is neglected.

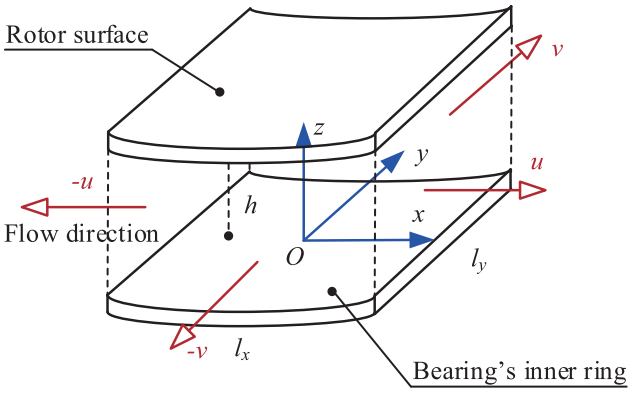

FIGURE 6. Expansion graph of the bearing's single-axis radiating surface.

Otherwise, the pressure in air film will not equals to ambient pressure constantly due to the air flowing state's change on the boundary. As shown in Fig. 5, pressure variation occurs at the position 1, 2, and 3. Actually, the air film in the gap makes squeezing movement under the excitation of the bearing inner ring's high-frequency vibration. One cycle of the squeezing movement can be divided two stages: a positive squeeze stage and a negative squeeze stage. At the positive squeeze stage shown in Fig. 5(a), the gas squirts out form the air gap to a free and open space along the straight line. In this case, the pressure in air film equals to ambient pressure. But at the negative squeeze stage shown in Fig. 5(b), ambient gas is sucked into a narrow and small space, and the flowing velocity instantly increases. Therefore, the pressure in the air film is smaller than the ambient pressure at this moment.

In the modeling of levitating force, the pressure variation Δp in the air film is taken into consideration. Therefore, we get

$$\begin{cases}p=p_0 & \dfrac{dh}{dt}<0\\ p=p_0-\Delta p & \dfrac{dh}{dt}>0\end{cases}\tag{18}$$

If the single-axis radiating surface on bearing inner ring and the corresponding overlapping rotor surface are unfolded in the circumferential direction, the structure shown in Fig. 6 is acquired. The characteristic length in x direction and in y direction are defined as l_x and l_y respectively. Some hypotheses are made: (1) air flow on the boundary is laminar flow; (2) the velocity change for the air on the boundary is continuous; (3) the sum of potential energy and kinetic energy is constant on the air flow line; (4) viscosity loss of air flow on the boundary is neglected. Based on above assumptions, when the air film in the gap makes squeezing movement, the quantity of air flowing through the boundary in unit time equals to the volume variation of the air film in the gap between the bearing and the rotor. Thus,

$$2l_x\int_0^h vdz+2l_y\int_0^h udz=-l_xl_y\frac{\mathrm{d}h}{\mathrm{d}t}\tag{19}$$

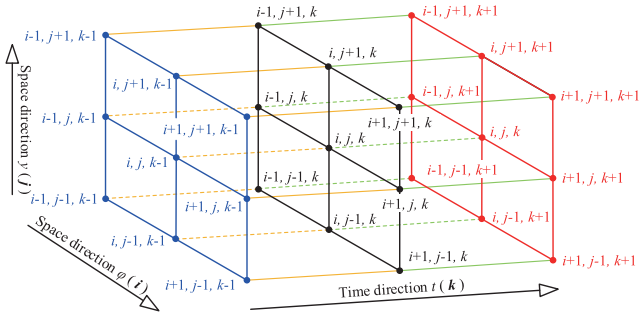

FIGURE 7. Mesh generation in space and time dimensions.

In the process of air flowing into or out from the air film, the mechanical energy is constant. According to the Bernoulli equation, we get

$$-\Delta p + \frac{1}{2}\rho v^2 = 0 \tag{20}$$

where $u \approx v \approx -\frac{l_x l_y (\mathrm{d}h/\mathrm{d}t)}{2(l_x+l_y)h}$

The equation set that consists of Eq.(19) and Eq.(20) is solved, and the pressure difference Δp is obtained.

$$\Delta p = \frac{1}{8}\rho \frac{{l_x}^2 {l_y}^2}{(l_x + l_y)^2}\left(\frac{1}{h}\frac{\mathrm{d}h}{\mathrm{d}t}\right)^2 \tag{21}$$

E. SOLUTION OF THE MODIFIED REYNOLDS EQUATION

The ultrasonic bearing's hydrodynamic equation is a kind of high-order multidimensional partial differential equation. For nonlinear partial differential equation, the finite difference method is an effective numerical method. General difference schemes include explicit difference scheme, implicit difference scheme and three-layer difference scheme like Du Fort-Frankel scheme etc [24]. Crank-Nicolson scheme is a kind of weighted implicit difference scheme. On account of its unconditional stability and relative high computational accuracy, this scheme is widespread used to solve the partial differential equations [25]–[27]. The first step of solving the differential equation Eq. (17) using finite difference method is the discretization of the definite solution region. Mesh generation in space and time dimensions is shown in Fig. 7.

The initial condition and boundary condition are given:

(1) initial condition: $P(\phi,\ Y,\ T=0)=1$

(2) boundary condition: $\begin{cases} P(\phi{=}0,\ Y,\ T)=1 \\ P(\phi{=}1/3,\ Y,\ T)=1 \\ P(\phi{=}2/3,\ Y,\ T)=1 \\ P(\phi,\ Y=\pm 1,\ T)=1 \end{cases}$

If we construct the finite difference scheme forward in time dimension, the following differential scheme is given

$$A_1 + B_1 + C_1 = D_1 + E \tag{22}$$

Otherwise, if we construct the finite difference scheme backward in time dimension, the following differential scheme is given

$$A_2 + B_2 + C_2 = D_2 + E \tag{23}$$

where the expression of $A_1, A_2, B_1, B_2, C_1, C_2, D_1, D_2$ and E are shown as follows.

Then, the weighted implicit difference scheme is established shown in Eq. (24).

$$\begin{aligned}(1-\Theta)(A_1 + B_1 + C_1 - D_1 - E) \\ + \Theta(A_2 + B_2 + C_2 - D_2 - E) = 0\end{aligned} \tag{24}$$

where Θ is the weighted value of the implicit difference scheme. When $\Theta = 0$ or $\Theta = 1$, the difference scheme shown in Eq. (24) becomes forward difference scheme or backward difference scheme respectively. When $\Theta = 1/2$ the difference scheme has second-order accuracy.

The computational flow chart of the above difference scheme is shown in Fig. 8. Calculation program is written using MATLAB software, and the pressure distribution in air film between the bearing and the rotor is figured out. After surface integral, the levitation force that the bearing acts on the rotor is acquired.

When the vibration amplitude of the bearing's inner ring is defined as 12.5 μm, and the vertical levitation height of the rotor is defined as 25 μm, the calculated pressure distribution in the air film is shown in Fig. 9. Fig. 9 (b), (c) and (d) represent the dimensionless pressure generated by the piezoelectric transducer PT-1, PT-2 and PT-3 respectively.

IV. THE STATIC AND DYNAMIC LEVITATION FORCE OF ULTRASONIC BEARING

When the rotor runs at a high speed, the levitation force generated by ultrasonic bearing is derived from two parts: one part is the acoustic radiation force generated by the high-frequency vibration of the bearing inner ring, and the other part is the hydrodynamic pressure generated by the high-speed rotor when the rotor is eccentric relative to the bearing's center line. If the dimensionless rotary speed U is set as zero, the calculated levitation force of Eq. (17) is static levitation force. While the dimensionless rotary speed U is not zero, the calculated levitation force of Eq. (17) is dynamic levitation force.

A. STATIC LEVITATION FORCE

In order to test the ultrasonic bearing's static radial levitation force, a measurement scheme shown in Fig. 10 is proposed. In the testing experiment, the rotor is fabricated as symmetrical structure. Two shaft shoulders are manufactured on the overhanging end of the rotor. The cylindrical surfaces of the shaft shoulders have high processing precision so that they can be used as measuring planes. Different levitating loads can be acquired through changing the mass of the weights hanging on both sides of the rotor. The displacement sensors are adopted to record the levitation heights under different loads. In the testing experiment, the rotor's center is on the middle plane, and the weights on the both sides are equal. To avoid the rotor's axial movement, two small air streams are generated by a air pump are used to keep the rotor's axial position. If the levitation heights getting from the displacement

$$A_1 = \frac{1}{2(\Delta\phi)^2}\left\{\begin{array}{l}\left[\begin{array}{l}k_{\varphi}{}^{k}_{i+1,j}(1-\frac{\rho_0 c^2}{\eta}\frac{P^k_{i+1,j}H^k_{i+1,j}}{4}\frac{\partial H^k_{i+1,j}}{\partial t})P^k_{i+1,j}{H^k_{i+1,j}}^3\\ +k_{\varphi}{}^{k}_{i,j}(1-\frac{\rho_0 c^2}{\eta}\frac{P^k_{i,j}H^k_{i,j}}{4}\frac{\partial H^k_{i,j}}{\partial t})P^k_{i,j}{H^k_{i,j}}^3\end{array}\right]\left(P^k_{i,j}-P^k_{i,j}\right)\\ -\left[\begin{array}{l}k_{\varphi}{}^{k}_{i,j}(1-\frac{\rho_0 c^2}{\eta}\frac{P^k_{i,j}H^k_{i,j}}{4}\frac{\partial H^k_{i,j}}{\partial t})P^k_{i,j}{H^k_{i,j}}^3\\ +k_{\varphi}{}^{k}_{i-1,j}(1-\frac{\rho_0 c^2}{\eta}\frac{P^k_{i-1,j}H^k_{i-1,j}}{4}\frac{\partial H^k_{i-1,j}}{\partial t})P^k_{i-1,j}{H^k_{i-1,j}}^3\end{array}\right]\left(P^k_{i,j}-P^k_{i,j}\right)\end{array}\right\}$$

$$B_1 = \frac{\pi^2 r^2 \rho_0 U}{p_0}\frac{1}{\Delta\phi}\left[k_{\varphi}{}^{k}_{i+1,j}{P^k_{i+1,j}}^2{H^k_{i+1,j}}^2\frac{\partial H^k_{i+1,j}}{\partial t}-k_{\varphi}{}^{k}_{i-1,j}{P^k_{i-1,j}}^2{H^k_{i-1,j}}^2\frac{\partial H^k_{i-1,j}}{\partial t}\right]$$

$$C_1 = \frac{1}{2(\Delta Y)^2}\left\{\begin{array}{l}\left[\begin{array}{l}k_{y}{}^{k}_{i,j+1}(1-\frac{\rho_0 c^2}{\eta}\frac{P^k_{i,j+1}H^k_{i,j+1}}{4}\frac{\partial H^k_{i,j+1}}{\partial T})P^k_{i,j+1}{H^k_{i,j+1}}^3\\ +k_{y}{}^{k}_{i,j}(1-\frac{\rho_0 c^2}{\eta}\frac{P^k_{i,j}H^k_{i,j}}{4}\frac{\partial H^k_{i,j}}{\partial T})P^k_{i,j}{H^k_{i,j}}^3\end{array}\right]\left(P^k_{i,j+1}-P^k_{i,j}\right)\\ -\left[\begin{array}{l}k_{y}{}^{k}_{i,j}(1-\frac{\rho_0 c^2}{\eta}\frac{P^k_{i,j}H^k_{i,j}}{4}\frac{\partial H^k_{i,j}}{\partial T})P^k_{i,j}{H^k_{i,j}}^3\\ +k_{y}{}^{k}_{i,j-1}(1-\frac{\rho_0 c^2}{\eta}\frac{P^k_{i,j-1}H^k_{i,j-1}}{4}\frac{\partial H^k_{i,j-1}}{\partial T})P^k_{i,j-1}{H^k_{i,j-1}}^3\end{array}\right]\left(P^k_{i,j}-P^k_{i,j-1}\right)\end{array}\right\}$$

$$D_1 = \frac{6\pi r\eta U}{p_0 c^2}\frac{1}{\Delta\phi}\left[k_{\varphi}{}^{k}_{i+1,j}P^k_{i+1,j}H^k_{i+1,j}-k_{\varphi}{}^{k}_{i-1,j}P^k_{i-1,j}H^k_{i-1,j}\right]$$

$$A_2 = \frac{1}{2(\Delta\phi)^2}\left\{\begin{array}{l}\left[\begin{array}{l}k_{\varphi}{}^{k+1}_{i+1,j}(1-\frac{\rho_0 c^2}{\eta}\frac{P^{k+1}_{i+1,j}H^{k+1}_{i+1,j}}{4}\frac{\partial H^{k+1}_{i+1,j}}{\partial t})P^{k+1}_{i+1,j}\left(H^{k+1}_{i+1,j}\right)^3\\ +k_{\varphi}{}^{k+1}_{i,j}(1-\frac{\rho_0 c^2}{\eta}\frac{P^{k+1}_{i,j}H^{k+1}_{i,j}}{4}\frac{\partial H^{k+1}_{i,j}}{\partial t})P^{k+1}_{i,j}\left(H^{k+1}_{i,j}\right)^3\end{array}\right]\left(P^{k+1}_{i,j}-P^{k+1}_{i,j}\right)\\ -\left[\begin{array}{l}k_{\varphi}{}^{k+1}_{i,j}(1-\frac{\rho_0 c^2}{\eta}\frac{P^{k+1}_{i,j}H^{k+1}_{i,j}}{4}\frac{\partial H^{k+1}_{i,j}}{\partial t})P^{k+1}_{i,j}\left(H^{k+1}_{i,j}\right)^3\\ +k_{\varphi}{}^{k+1}_{i-1,j}(1-\frac{\rho_0 c^2}{\eta}\frac{P^{k+1}_{i-1,j}H^{k+1}_{i-1,j}}{4}\frac{\partial H^{k+1}_{i-1,j}}{\partial t})P^{k+1}_{i-1,j}\left(H^{k+1}_{i-1,j}\right)^3\end{array}\right]\left(P^{k+1}_{i,j}-P^{k+1}_{i,j}\right)\end{array}\right\}$$

$$B_2 = \frac{\pi^2 r^2 \rho_0 U}{p_0}\frac{1}{\Delta\phi}\left[k_{\varphi}{}^{k+1}_{i+1,j}\left(P^{k+1}_{i+1,j}H^{k+1}_{i+1,j}\right)^2\frac{\partial H^{k+1}_{i+1,j}}{\partial t}-k_{\varphi}{}^{k+1}_{i-1,j}\left(P^{k+1}_{i-1,j}H^{k+1}_{i-1,j}\right)^2\frac{\partial H^{k+1}_{i-1,j}}{\partial t}\right]$$

$$C_2 = \frac{1}{2(\Delta Y)^2}\left\{\begin{array}{l}\left[\begin{array}{l}k_{y}{}^{k+1}_{i,j+1}(1-\frac{\rho_0 c^2}{\eta}\frac{P^{k+1}_{i,j+1}H^{k+1}_{i,j+1}}{4}\frac{\partial H^{k+1}_{i,j+1}}{\partial T})P^{k+1}_{i,j+1}\left(H^{k+1}_{i,j+1}\right)^3\\ +k_{y}{}^{k+1}_{i,j}(1-\frac{\rho_0 c^2}{\eta}\frac{P^{k+1}_{i,j}H^{k+1}_{i,j}}{4}\frac{\partial H^{k+1}_{i,j}}{\partial T})P^{k+1}_{i,j}\left(H^{k+1}_{i,j}\right)^3\end{array}\right]\left(P^{k+1}_{i,j+1}-P^{k+1}_{i,j}\right)\\ -\left[\begin{array}{l}k_{y}{}^{k+1}_{i,j}(1-\frac{\rho_0 c^2}{\eta}\frac{P^{k+1}_{i,j}H^{k+1}_{i,j}}{4}\frac{\partial H^{k+1}_{i,j}}{\partial T})P^{k+1}_{i,j}\left(H^{k+1}_{i,j}\right)^3\\ +k_{y}{}^{k+1}_{i,j-1}(1-\frac{\rho_0 c^2}{\eta}\frac{P^{k+1}_{i,j-1}H^{k+1}_{i,j-1}}{4}\frac{\partial H^{k+1}_{i,j-1}}{\partial T})P^{k+1}_{i,j-1}\left(H^{k+1}_{i,j-1}\right)^3\end{array}\right]\left(P^{k+1}_{i,j}-P^{k+1}_{i,j-1}\right)\end{array}\right\}$$

$$D_2 = \frac{6\pi r\eta U}{p_0 c^2}\frac{1}{\Delta\phi}\left[k_{\varphi}{}^{k+1}_{i+1,j}P^{k+1}_{i+1,j}H^{k+1}_{i+1,j}-k_{\varphi}{}^{k+1}_{i-1,j}P^{k+1}_{i-1,j}H^{k+1}_{i-1,j}\right]$$

$$E = \frac{48\pi^2 r^2\eta}{p_0 c^2}\frac{P^{k+1}_{i,j}H^{k+1}_{i,j}-P^k_{i,j}H^k_{i,j}}{\Delta T}$$

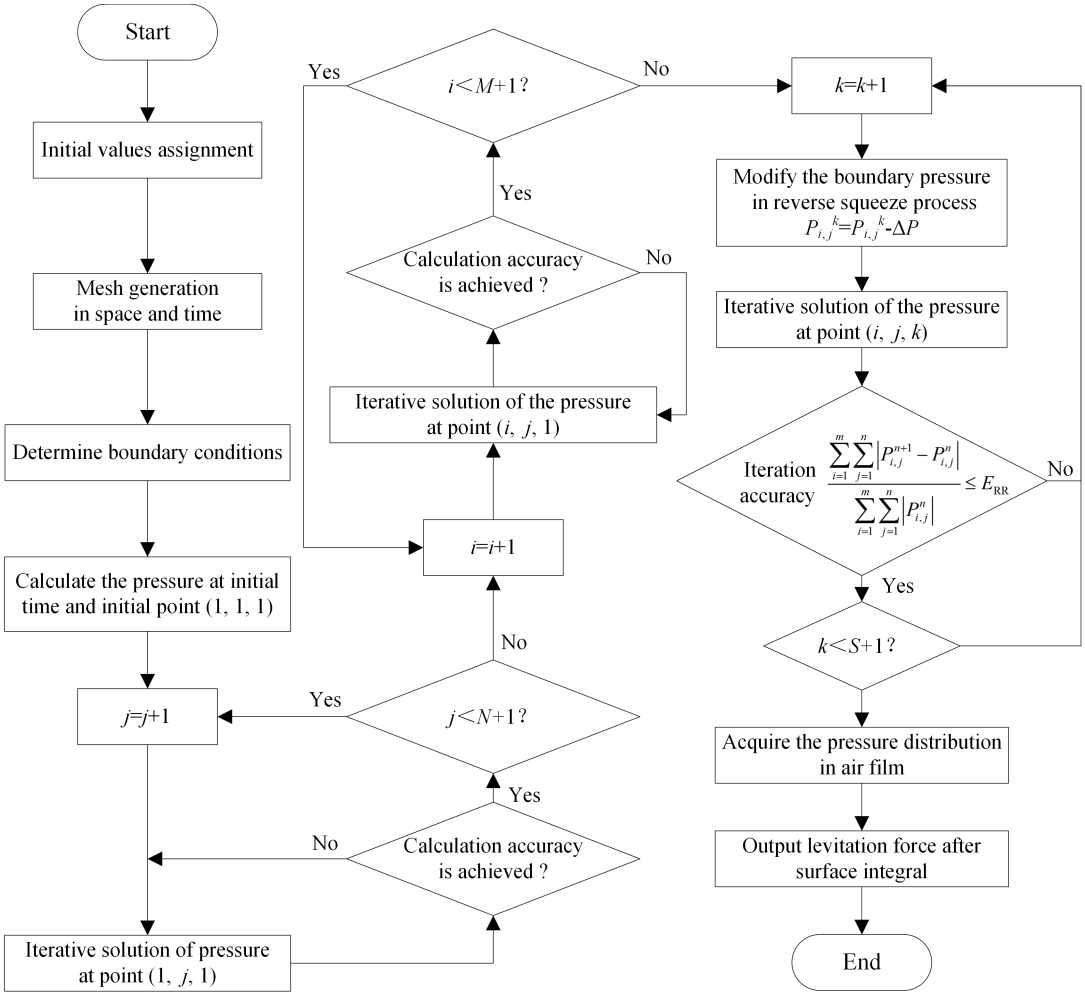

FIGURE 8. Flow chart of the solution procedure of the bearing's hydrodynamic equation.

sensor 1 and sensor 2 are h_{s1} and h_{s2} respectively, the rotor's levitation height is $h_s = h_{s1} + h_{s2}$. This measurement method eliminates the error caused by the lean of the rotor's central axis.

The diameter clearance between the ultrasonic bearing and the rotor used in the experiment is 90 μm. The excitation voltages of the three piezoelectric transducers are all 150 V (peak-to-peak value), at this moment, the output vibration amplitudes of the transducers are 12.5 μm. The testing experiments are conducted in a closed dustless room. The temperature in the room is controlled in the range from 18 °C to 22 °C, and the humidity is 55 $\pm$ 10%. The repeatability error and precision of the laser sensor are 0.02 μm and 1.2 μm, respectively.

Table 1 lists the ultrasonic bearing's static levitation forces under different vertical levitation heights. 30-group experiments are designed and the each group consists of five experiments. The experimental result is the average value of every group experiment. Fig. 11 presents the comparison of the theoretical and experimental results, and the deviation is also calculated which listed in Table 1.

The comparison between the theoretical and experimental results illustrates that the levitation force of the bearing declines as the levitation height increases from 15 μm to 45 μm, and the descending rate gradually becomes slow. When the levitation height reduces from 15 μm to the bearing inner ring's vibration amplitude, the leviation force rapidly increases. In this case, the piezoelectric transducer PT-1 acts a dominant role on the bearing's load-carrying capacity, but the levitation effect generated by transducers PT-2 and PT-3 is small. When the levitation height increases to 45 μm, that is, the rotor's center axis coincides with the bearing inner ring's center axis, the static levitation force is close to zero. When the vertical levitation height exceeds 45 μm, the bearing will generate a radial levitation force downward. Through analysis on the experimental data's deviation from theoretical results, it is found that the theoretical curve can interpret the experimental data when the levitation height 15 μm$< h_0 <$ 20 μm. But when 20 μm$< h_0 <$ 45 μm,

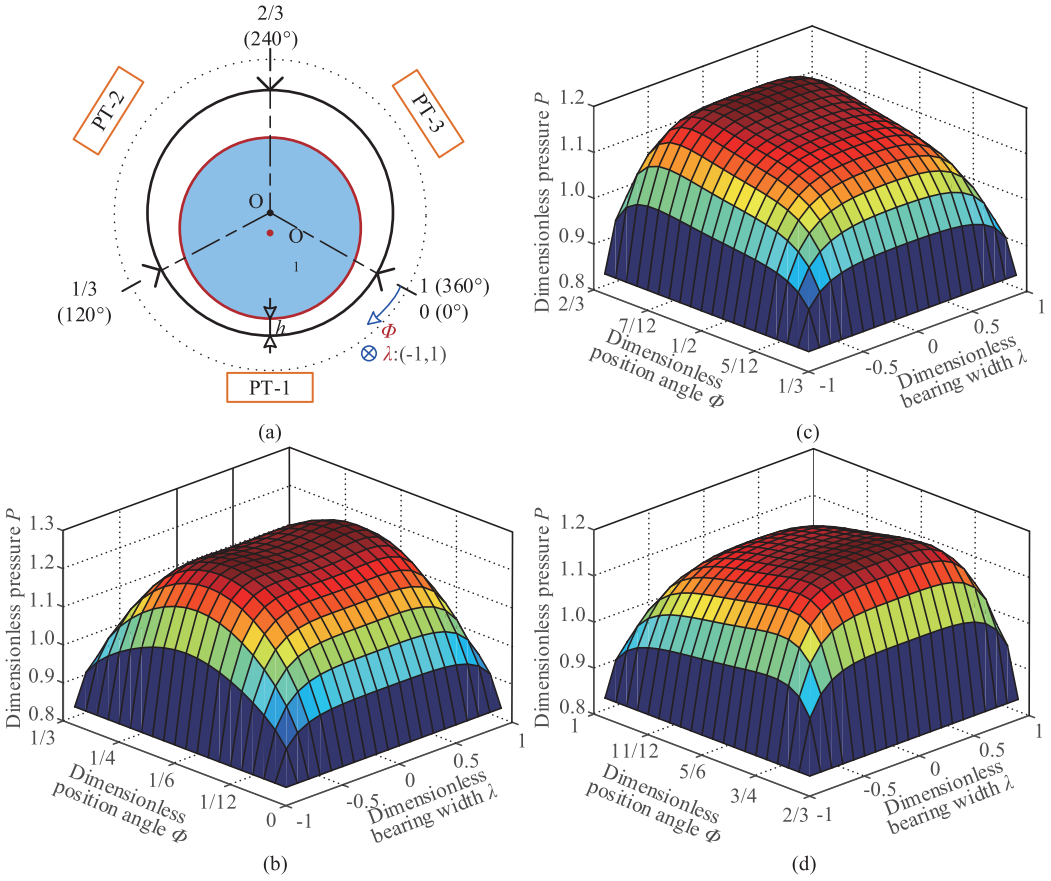

FIGURE 9. Sound pressure distribution in the air film of the bearing when the levitation height is 25 μm. (a) Bearing's schematic diagram. (b) Pressure distribution of PT-1. (c) Pressure distribution of PT-2. (d) Pressure distribution of PT-3.

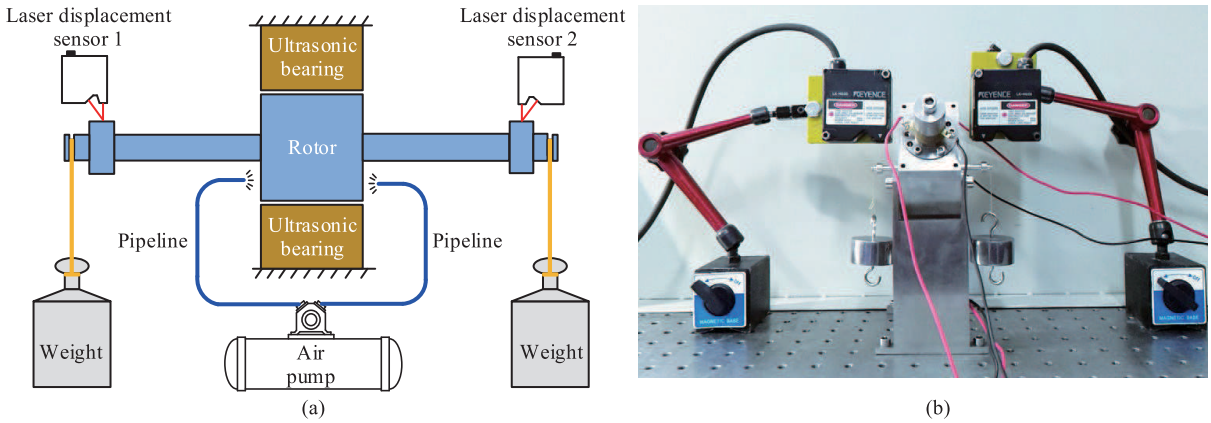

FIGURE 10. Measuring principle of radial levitation force of the three-axis levitating bearing. (a) Measurement principle. (b) Experimental device diagram.

there is a difference between the theoretical and experimental results. That is due to that the eccentric distance of the rotor is relatively small and the radial levitation force on the rotor is smaller and more susceptible to the external disturbance. Moreover, the levitation force are inevitably subjected to the effect of gas film oscillation in this case.

B. DYNAMIC LEVITATION FORCE

When the rotor in the eccentric state runs at a high speed, the ultrasonic bearing's levitation force is derived from the near-field acoustic levitation effect and the hydrodynamic pressure effect. Synthetic action of near field acoustic levitation effect and hydrodynamic effect is shown in Fig. 12. According to the established levitation force model shown

TABLE 1. Theoretical and experimental data of the bearing's levitation force.

Expt. group No.	Levitating height avg. value (μm)	Levitating force theor. value (N)	Levitating force expt. value (N)	Deviation (%)
1	42.9	0.171	0.235	27.23
2	37.1	0.680	0.431	57.77
3	35.9	0.871	0.627	38.92
4	34.3	1.068	0.823	29.77
5	32.3	1.270	1.215	4.52
6	31.2	1.469	1.411	4.11
7	29.4	1.812	1.803	0.50
8	27.8	2.085	2.195	5.01
9	27.1	2.204	2.587	14.80
10	25.1	2.682	2.979	9.97
11	23.1	3.184	3.175	0.28
12	21.8	3.594	3.371	6.62
13	21.4	3.722	3.763	1.09
14	20.4	4.160	4.155	0.12
15	19.6	4.541	4.547	0.13
16	18.9	4.926	4.939	0.26
17	17.8	5.613	5.331	5.29
18	17.6	5.787	5.723	1.12
19	16.9	6.374	6.311	1.00
20	16.6	6.685	6.703	0.27
21	16.2	7.046	7.095	0.69
22	15.7	7.574	7.487	1.16
23	15.5	8.010	7.879	1.66
24	15.1	8.508	8.467	0.48
25	14.8	8.871	8.859	0.14
26	14.6	9.502	9.447	0.58
27	14.2	9.977	10.035	0.58
28	14.0	10.485	10.819	3.09
29	13.6	11.009	11.015	0.05
30	13.5	11.582	11.603	0.18

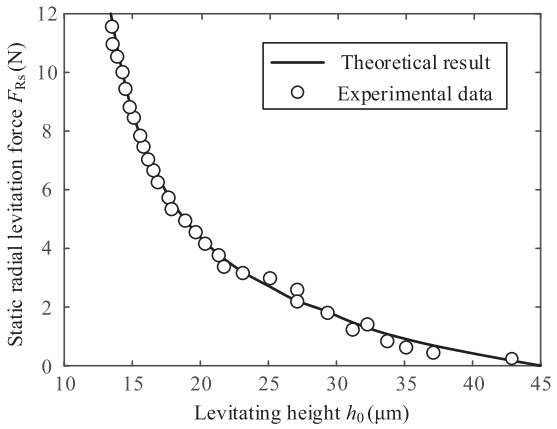

FIGURE 11. Comparison between theoretical and experimental results of radial levitation force.

in Eq. (17), it is known that the levitation force is not the simple superposition of the radiation force and the hydrodynamic pressure but the result of coupling of the two effects.

The dynamic levitation force testing experiment is difficult to conducted when the rotor runs at high speeds. To reveal the hydrodynamic effect's role in the bearing's levitation force, the theoretical analysis based on the levitation model is a feasible and effective method. During the process of calculation, the radial clearance between the ultrasonic bearing and the rotor is set as 45 μm. The output vibration amplitude of the bearing's inner ring is 12.5 μm. The working medium used in the model is air. If the rotary speed increases from 0 r/min to 100000 r/min, the leviation force's changing rule is obtained when the levitation heights are 15 μm, 25 μm, 35 μm and 45 μm respectively. The calculation results are shown in Fig. 13. The curves illustrate that the levitation forces increase by 0.03 N, 0.007 N, 0.00085 N and 0 N for radial clearance of 15 μm, 25 μm, 35 μm and 45 μm, respectively. From the calculated results, it is clearly seen that the greater the eccentricity is, the more significant the effect becomes. When the leviation height is 45 μm, in this case, there is no eccentricity for the rotor, thus the leviation force is only provided by the near-field acoustic levitation effect. Since the viscosity of air is low (its order of magnitude is usually 10^{-5} Pa·s at room temperature and normal atmospheric pressure conditions), the hydrodynamic pressure is two orders smaller than the gas film force as the rotary speed is less than 10^5 r/min. Therefore, the gas film force plays a dominant role in the process of supporting the loads. Although the proportion of hydrodynamic pressure among radial levitation force is small, the hydrodynamic effect will contribute to the bearing's self-aligning capability when the bearing runs at a high speed.

V. INFLUENCE FACTORS ON LEVITATION FORCE

In addition to rotary speed, there are several factors affecting the bearing's levitation force. These factors include piezoelectric transducer's dynamic parameters, working medium, bearing's clearance size, environmental temperature and humidity, etc. The analysis of these factors' impact on ultrasonic bearing's levitation force will provide guidance for the bearing's design, selection of working media and control of bearing's working environment.

A. DYNAMIC PARAMETERS' EFFECT ON LEVITATION FORCE

Piezoelectric transducer is the excitation element of ultrasonic bearing inner ring's vibration. The major parameters such as resonant frequency and output amplitude exert a significant effect on the bearing's levitation force. According to the ultrasonic bearing's levitation force model, the levitation force's change with time in a period is calculated when the resonant frequencies are 5 kHz, 10 kHz, 15 kHz, 20 kHz and 25 kHz, respectively. From the calculated results shown in Fig. 14(a), it is found that the time-averaged levitation forces in one period are 3.632 N, 3.459 N, 2.473 N, 1.626 N and 1.433 N at the resonant frequencies of 5 kHz, 10 kHz, 15 kHz, 20 kHz and 25 kHz, respectively. In the frequency domain of 0−30 kHz, the bearing's levitation force's variation with frequency is acquired. It is clearly seen from the curve shown in Fig. 14(b), the levitation force climbs up and then decline until it tends to a stable value. When the resonant frequency is 7 kHz, the levitation force reaches to maximum value. In the bearing's design process, the noise produced by the bearing should taken into account in addition

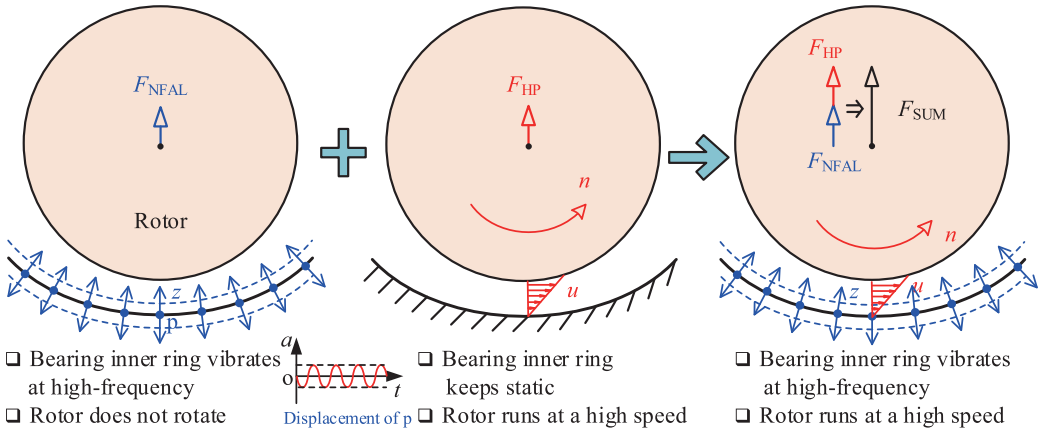

FIGURE 12. Principle of combined action of near field acoustic levitation effect and hydrodynamic effect.

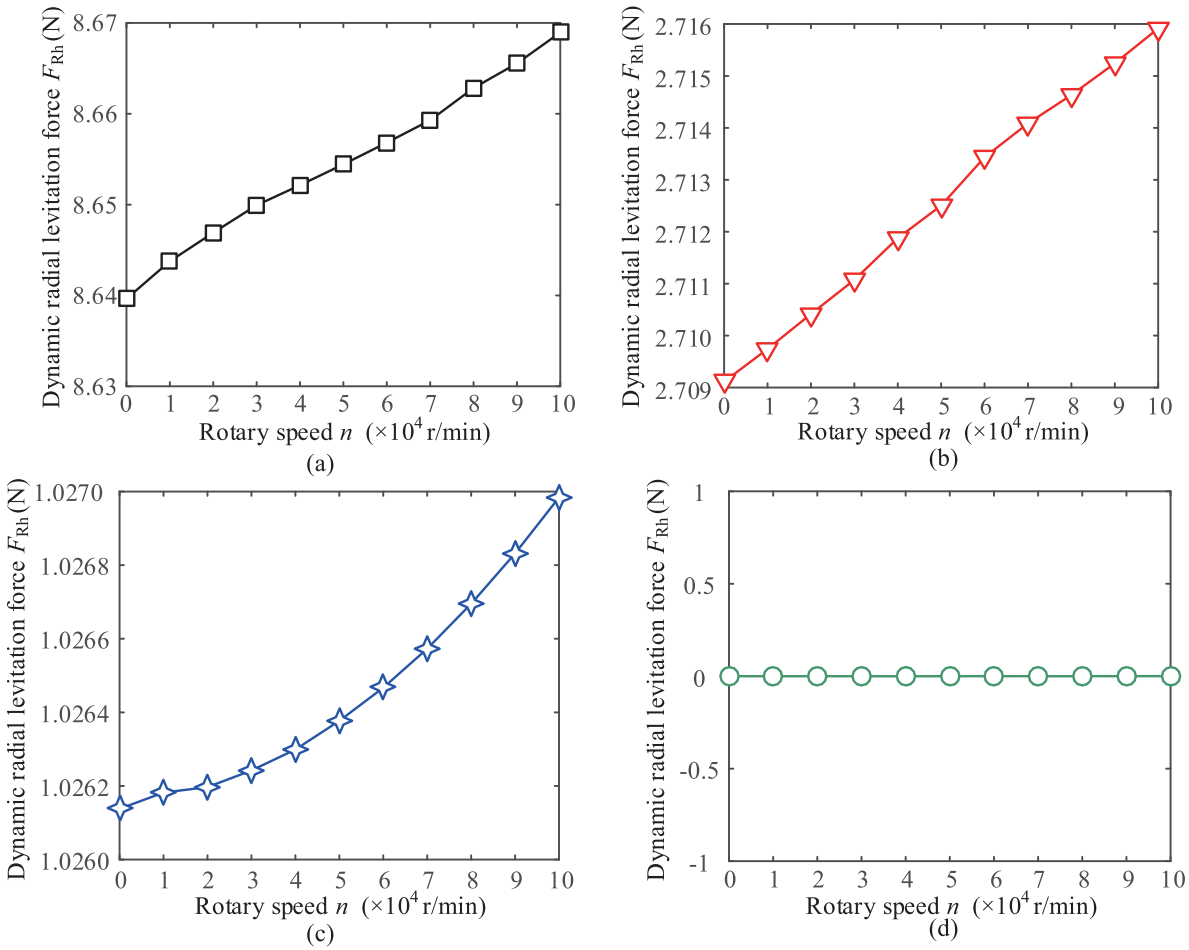

FIGURE 13. Relation between the radial levitation force and rotary speed under different levitation heights. (a) h=15 μm. (b) h=25 μm. (c) h=35 μm. (d) h=45 μm.

to the bearing's load-carrying capacity. When the bearing operates at a frequency less than 16 kHz, the bearing will produce loud noises. If the bearing operates at the frequency of 16 kHz, the bearing's noise level reduces to 20 dB. When load-carrying capacity and noise level are considered together, a design value of frequency within 16−20 kHz is more reasonable.

Since the transducers' radiation surfaces form the ultrasonic bearing's inner ring, the vibration amplitude of the bearing's inner ring is the output vibration amplitude of the

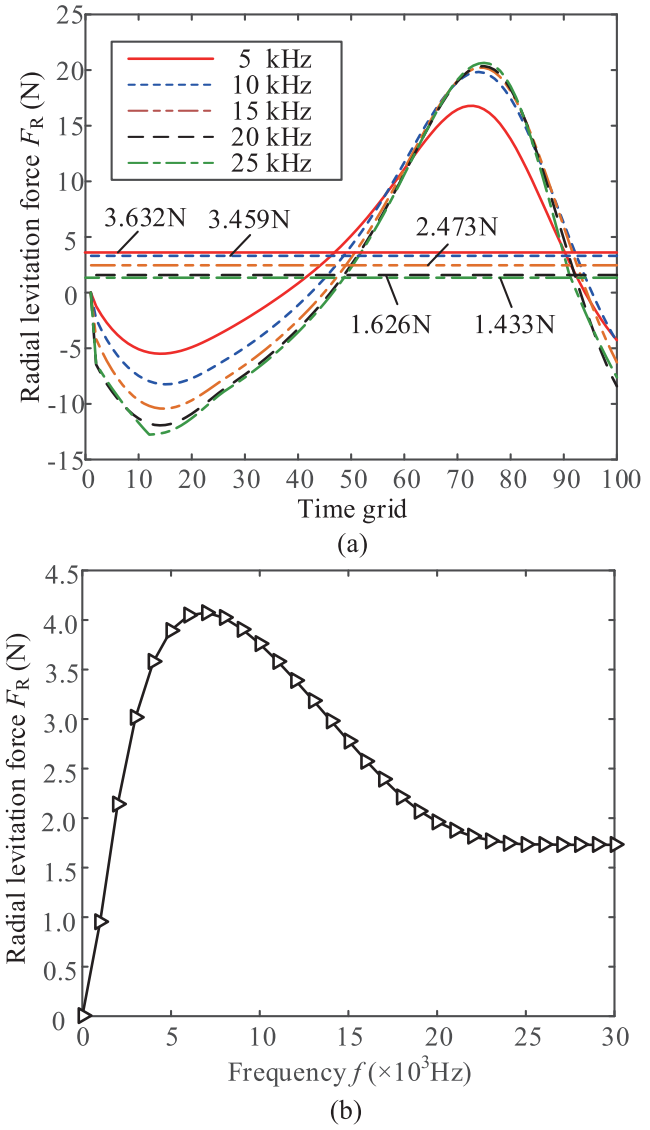

FIGURE 14. Relation between the radial levitation force and resonant frequency. (a) The time-averaged levitation forces at different resonant frequencies. (b) The levitation force's variation with frequency.

transducers. To investigate the vibration amplitude's impact on the levitation force, the levitation force's change rule is calculated under different levitation heights (15 μm, 20 μm, 25 μm, 30 μm and 35 μm) when vibration amplitude varies from 0 to 20 μm. The results shown in Fig. 15 demonstrate that the levitation force raises as the vibration amplitude increases, and the rate of increase is getting faster and faster. According to the comparison among the five curves,it is also found that the vibration amplitude's influence on levitation force is more remarkable when levitation height is smaller.

Raising the vibration amplitude is a significant and effective method to improve the bearing's levitation effect. However, on account of that the increase of the amplitude of bearing's inner ring will give rise to the enlargement of the clearance between the bearing and rotor, the improvement of bearing's levitation effect by increasing vibration amplitude

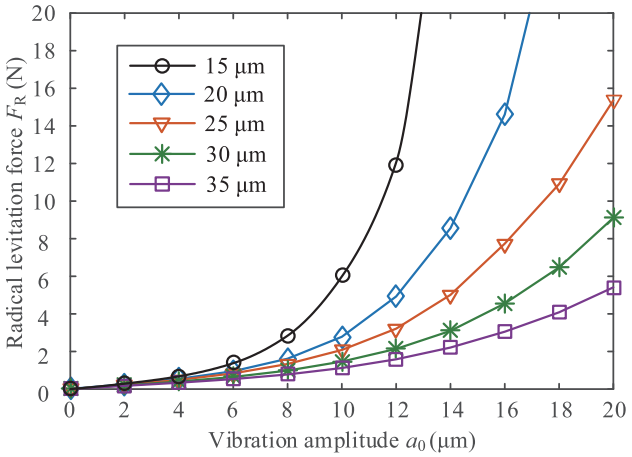

FIGURE 15. The curve of vibration amplitude's impact on the levitation force.

TABLE 2. Values of density and viscosity of some familiar gases under an atmospheric pressure of 100 kPa and a temperature of 25 °C.

Gas No.	Density ρ (kg/m^3)	Dynamic viscosity η (μPa·s)
1	0.081	8.915
2	0.814	31.113
3	1.130	17.805
4	1.169	18.448
5	1.292	20.550
6	1.613	22.624
7	1.784	14.932

is at the cost of sacrificing the kinematic accuracy of the bearing. Therefore, the vibration amplitude's design need to balance the levitation effect and kinematic accuracy. Moreover, the manufacturing precision and machined surface quality of the bearing and rotor should be taken into account.

B. WORKING MEDIUM'S EFFECT ON LEVITATION FORCE

Different working media used in ultrasonic bearing have different physical and mechanical properties. Working medium's selection will also affect the bearing's levitation effect. Among the gas's physical and mechanical properties, the density and dynamic viscosity are two leading factors influencing the bearing's levitation effect. Some common gases' density and viscosity under an atmospheric pressure of 100 kPa and a temperature of 25 °C are listed in Table 2.

After calculation, the levitation forces under different levitation heights are acquired for above 7 kinds of working media. The levitation force curves shown in Fig. 16 reveal that the levitation force is maximum for gas no.1 but minimum for gas no.7. It is believed that the larger the gas's density is, the more remarkable the inertia effect and boundary effect become. The density of gas 1 is about one twentieth of gas 7's density, thus the pressure loss caused by inertia and boundary effect is much smaller. With regard to above 7 gases, the dynamic viscosities are in an order of μPa·s, the influence

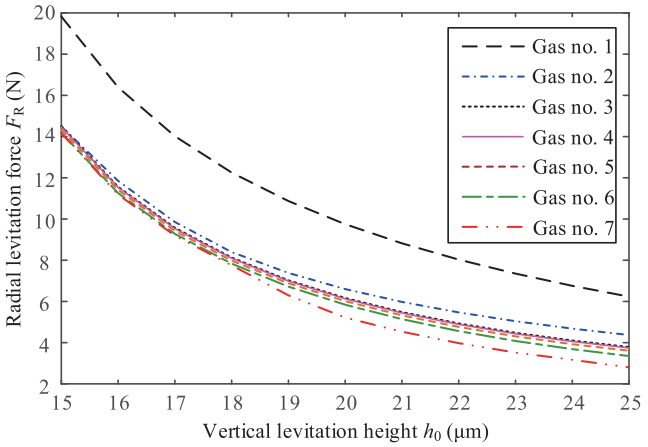

FIGURE 16. Levitation forces under different levitation heights for different kinds of working media.

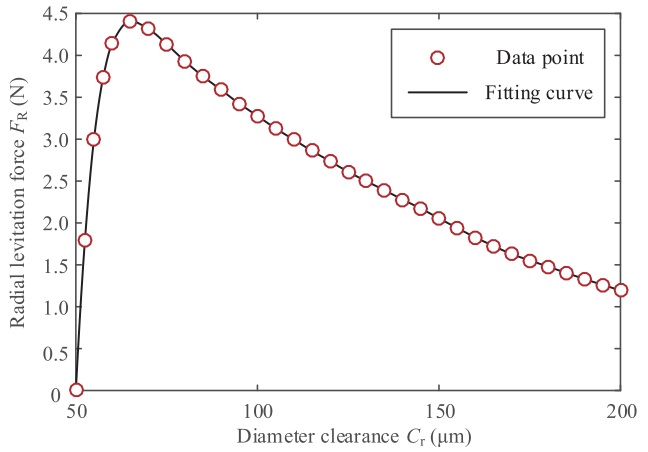

FIGURE 17. The relation between the levitation force and bearing's clearance.

of viscosity on levitation force is smaller than that of density. For gas 3, gas 4 and gas 5, since their density and viscosity values are close to each other, the levitation force values are also similar.

C. BEARING CLEARANCE'S EFFECT ON LEVITATION FORCE

When piezoelectric transducer's output characteristics, bearing's working medium and levitation height all remain constant values, the bearing's clearance will exert a big impact on levitation force. The relation between the levitation force and bearing's clearance is studied when the bearing inner ring's vibration amplitude is 12.5 μm and the levitation height is 25 μm. The relation curve is shown in Fig. 17. The curve indicates that there is a sharp increase for levitation force when the diameter clearance ranges from 50 μm to 65 μm. If the diameter clearance is 50 μm, the rotor center axis coincides with the bearing inner ring's center axis. In this case, the levitation force is zero. When the diameter clearance is 65 μm, the levitation force reaches to maximum. When the diameter clearance exceeds 65 μm, the levitation force will slowly reduce to zero with the rise of diameter clearance.

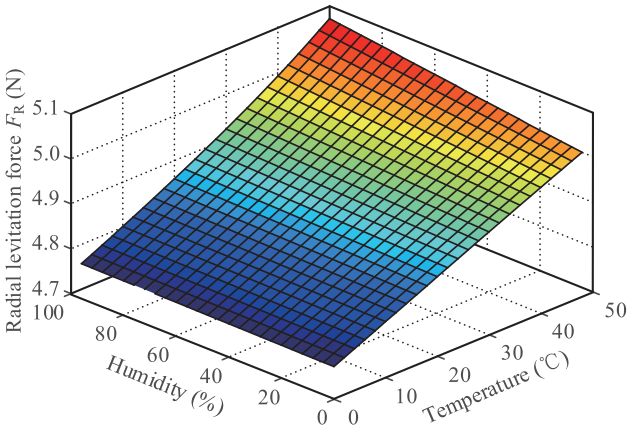

FIGURE 18. The levitation force's changing rule with temperature and humidity.

D. AMBIENT TEMPERATURE AND RELATIVE HUMIDITY'S EFFECT ON LEVITATION FORCE

In addition to above mentioned influencing factors, the temperature and humidity of the bearing's working environment are vital factors that can not be neglected. The ambient temperature and humidity have a great effect on the gas's physical property parameters. The change of the gas's physical property parameters will affect the bearing's levitation force.

Air is the most commonly used working medium for ultrasonic bearings. The air always contains a certain amount of vapor. According to properties of mixed gases, the density of moist air ρ_m is the sum of the dry air's density ρ_d and vapor's density ρ_v under same temperature and respective partial pressure. Thus,

$$\rho_m = \rho_d + \rho_v = \frac{P_m}{R_d T_h}\left[1 - \frac{R_v - R_d}{R_v}\frac{\psi P_s(t_0)}{P_m}\right] \quad (25)$$

where P_m, t_0 and T_h represent the moist air's pressure, Celsius temperature and Kelvin temperature, respectively. R_v and R_d are the vapor and dry air's gas constants. ψ is the relative humidity. $P_s(t_0)$ is the saturation vapor pressure at a temperature of t_0. The value of $P_s(t_0)$ can be calculated by the fitting formula: $P_s(t_0) = \exp(6.42 + 0.072t_0 - 0.000271t_0^2 + 7.23 \times 10^{-7}t_0^3)$.

The dynamic viscosity of the moist air η_m can be expressed as

$$\eta_m = \frac{Y_d M_{rd}^{1/2}\eta_d + Y_v M_{rv}^{1/2}\eta_v}{Y_d M_{rd}^{1/2} + Y_v M_{rv}^{1/2}} \quad (26)$$

where M_{rd} and M_{rv} are the dry air and vapor's relative molecular weights, Y_d and Y_v are the dry air and vapor's volume percentages, and the η_d and η_v are the dry air and vapor's dynamic viscosities. The values of η_d and η_v can be calculated by the following fitting formulas: $\eta_d = (17.4945 + 0.04779t_0 - 3.5256 \times 10^{-5}t_0^2) \times 10^{-6}$; $\eta_v = (8.1804 + 0.04011t_0 - 1.7858 \times 10^{-5}t_0^2) \times 10^{-6}$.

It is found from the Eq. (25) and Eq. (26) that the moist air's density and dynamic viscosity increase with the increase

of temperature within a range of 0−50 °C. But the moist air's density and dynamic viscosity decrease with the increase of the humidity. If the the moist air's density and dynamic viscosity values are substituted into the ultrasonic bearing's dynamics model, the bearing's levitation force's changing rule with temperature and humidity will be acquired when the moist air is used as the bearing's working medium. The calculated results are shown in Fig. 18. The two-dimensional surface diagram indicates that the bearing's levitation force grows with the increase of temperature and humidity. Thus, the bearing has a good levitating effect in the air with relative high temperature and large humidity.

VI. CONCLUSION

In this work, a new method for the prediction of the ultrasonic bearing's load-carrying capacity is presented. The proposed model takes gas inertia force, surface topography, rarefaction effect and boundary effect into account, and actually reflects the ultrasonic bearing's operation state. A measurement scheme for testing the bearing's static levitation force is designed, and the experiment results demonstrate that global average deviation of the calculated theoretical values is only 7.25%.

It is found from the theoretical model that the bearing's levitation effect on the rotor is derived from the combined action of near-field acoustic levitation effect and hydrodynamic effect when the rotor runs in an eccentricity state at a high speed. Although the proportion of hydrodynamic pressure is much smaller than that of near-field acoustic levitation force in the bearing's levitation force, its contribution to the bearing's self-aligning capability should be noticeable.

Based on the theoretical analysis and numerical results presented in the paper, some key factors influencing the ultrasonic bearing's levitation effect are investigated. We found that a frequency within a range of 16−20 kHz is a reasonable design value if comprehensively considering the load-carrying capacity and noise level of the bearing. The increasing vibration amplitude of bearing's inner ring is an effective method to improve the bearing's levitation effect, but the vibration amplitude's improvement should match the bearing clearance's design and meet the requirement of the bearing's kinematic accuracy. The air is a common medium for ultrasonic bearings. We also found that the bearing has a good levitating effect in the air with relative high temperature and large humidity.

The investigation of the ultrasonic bearing's levitation effect and the analysis on key factors influencing the bearing's levitation effect can guide the ultrasonic bearing's structural design and the selection of the ultrasonic bearing's working parameters, and accelerate the ultrasonic bearing's engineering application process.

REFERENCES

[1] B. Han, S. Zheng, Y. Le, and S. Xu, "Modeling and analysis of coupling performance between passive magnetic bearing and hybrid magnetic radial bearing for magnetically suspended flywheel," *IEEE Trans. Magn.*, vol. 49, no. 10, pp. 5356–5370, Oct. 2013.

[2] A. Boudinar, N. Benouzza, A. Bendiabdellah, and M. Khodja, "Induction motor bearing fault analysis using a root-MUSIC method," *IEEE Trans. Ind. Appl.*, vol. 52, no. 5, pp. 3851–3860, Sep./Oct. 2016.

[3] L. Smolik, M. Hajžman, and M. Byrtus, "Investigation of bearing clearance effects in dynamics of turbochargers," *Int. J. Mech. Sci.*, vol. 127, pp. 62–72, Jul. 2017.

[4] S. Kasolang, D. I. Ahmed, R. Dwyer-Joyce, and B. F. Yousif, "Performance analysis of journal bearings using ultrasonic reflection," *Tribology Int.*, vol. 64, no. 3, pp. 78–84, Aug. 2013.

[5] H. Li, Q. Quan, Z. Deng, D. Bai, and Y. Wang, "Design and experimental study on an ultrasonic bearing with bidirectional carrying capacity," *Sens. Actuators A, Phys.*, vol. 273, no. 3, pp. 58–66, Apr. 2018.

[6] T. Stolarski, R. Gawarkiewicz, and K. Tesch, "Extended duration running and impulse loading characteristics of an acoustic bearing with enhanced geometry," *Tribol. Lett.*, vol. 65, no. 2, pp. 1–8, Mar. 2017.

[7] S. Yoshimoto, H. Kobayashi, and M. Miyatake, "Float characteristics of a squeeze-film air bearing for a linear motion guide using ultrasonic vibration," *Tribology Lett.*, vol. 40, no. 3, pp. 503–511, Mar. 2007.

[8] C. Wang and Y. H. J. Au, "Study of design parameters for squeeze film air journal bearing—Excitation frequency and amplitude," *Mech. Sci.*, vol. 2, no. 2, pp. 147–155, Jul. 2011.

[9] H. Li and Z. Deng, "Experimental study on friction characteristics and running stability of a novel ultrasonic levitating bearing," *IEEE Access*, vol. 6, pp. 21719–21730, 2018.

[10] H. Nomura, T. Kamakura, and K. Matsuda, "Theoretical and experimental examination of near-field acoustic levitation," *J. Acoust. Soc. Amer.*, vol. 111, no. 4, pp. 1578–1583, Nov. 2002.

[11] P. Liu, J. Li, H. Ding, and W. Cao, "Modeling and experimental study on near-field acoustic levitation by flexural mode," *IEEE Trans. Ultrason., Ferroelectr., Freq. Control*, vol. 56, no. 12, pp. 2679–2685, Dec. 2009.

[12] J. Li, P. Liu, H. Ding, and W. Cao, "Modeling characterization and optimization design for PZT transducer used in Near Field Acoustic Levitation," *Sens. Actuators A, Phys.*, vol. 171, no. 2, pp. 260–265, Nov. 2011.

[13] J. Li, W. Cao, P. Liu, and H. Ding, "Influence of gas inertia and edge effect on squeeze film in near field acoustic levitation," *Appl. Phys. Lett.*, vol. 96, Jun. 2010, Art. no. 243507.

[14] J. Hu, K. Nakamura, and S. Ueha, "Stability analysis of an acoustically levitated disk," *IEEE Trans. Ultrason., Ferroelectr., Freq. Control*, vol. 50, no. 2, pp. 117–127, Feb. 2003.

[15] S. Zhao and J. Wallaschek, "A standing wave acoustic levitation system for large planar objects," *Arch. Appl. Mech.*, vol. 81, no. 2, pp. 123–139, Feb. 2011.

[16] S. Zhao, S. Mojrzisch, and J. Wallaschek, "An ultrasonic levitation journal bearing able to control spindle center position," *Mech. Syst. Signal Process.*, vol. 36, no. 1, pp. 168–181, Mar. 2013.

[17] T. A. Stolarski, R. Gawarkiewicz, and K. Tesch, "Acoustic journal bearing—A search for adequate configuration," *Tribology Int.*, vol. 92, pp. 387–394, Dec. 2005.

[18] T. A. Stolarski, "Running characteristics of aerodynamic bearing with self-lifting capability at low rotational speed," *Adv. Tribology*, vol. 2011, Mar. 2011, Art. no. 973740.

[19] T. A. Stolarski, R. Gawarkiewicz, and K. Tesch, "Acoustic journal bearing—Performance under various load and speed conditions," *Tribology Int.*, vol. 102, pp. 297–304, Oct. 2016.

[20] C. Chen, J. Wang, B. Jia, and F. Li, "Design of a noncontact spherical bearing based on near-field acoustic levitation," *J. Intell. Mater. Syst. Struct.*, vol. 25, no. 6, pp. 755–767, Nov. 2014.

[21] S. Shen, R. Yang, G. Chen, R. M. Crone, and M. Anaya-Dufresne, "Nonlocal formulation of the Reynolds equation for rarefied gas flow with steep pressure variation," *J. Appl. Phys.*, vol. 107, no. 10, May 2010, Art. no. 104316.

[22] A. Pandey and R. Pratap, "Coupled nonlinear effects of surface roughness and rarefaction on squeeze film damping in MEMS structures," *J. Micromech. Microeng.*, vol. 14, no. 10, pp. 1430–1437, Jul. 2004.

[23] A. K. Pandey, R. Pratap, and F. S. Chau, "Effect of pressure on fluid damping in MEMS torsional resonators with flow ranging from continuum to molecular regime," *Experim. Mech.*, vol. 48, no. 1, pp. 91–106, 2008.

[24] J. Crank and P. Nicolson, "A practical method for numerical evaluation of solutions of partial differential equations of the heat-conduction type," *Adv. Comput. Math.*, vol. 6, no. 1, pp. 207–226, Dec. 1996.

[25] G. Sun and C. W. Trueman, "Unconditionally stable Crank-Nicolson scheme for solving two-dimensional Maxwell's equations," *Electron. Lett.*, vol. 39, pp. 595–597, Apr. 2003.

[26] C. Reisinger and A. Whitley, "The impact of a natural time change on the convergence of the Crank-Nicolson scheme," *IMA J. Numer. Anal.*, vol. 34, no. 3, pp. 1156–1192, Sep. 2013.
[27] Y. He and J. Li, "Numerical implementation of the Crank–Nicolson/Adams–Bashforth scheme for the time-dependent Navier–Stokes equations," *Int. J. Numer. Methods Fluids*, vol. 62, no. 6, pp. 647–659, Feb. 2010.

HE LI was born in Shandong, China, in 1987. He received the B.S. degree in mechanical engineering from the Changchun University of Science and Technology, Changchun, China, in 2010, and the M.S. and Ph.D. degrees in mechanical engineering from the Harbin Institute of Technology, Harbin, China, in 2013 and 2018, respectively. He is currently a Lecturer with the College of Mechanical and Electronic Engineering, Shandong University of Science and Technology. His research interest includes ultrasonic bearings.

ZONGQUAN DENG was born in 1956. He received the B.S. and M.S. degrees from the Harbin Institute of Technology, Harbin, China, in 1982 and 1984, respectively. He is currently a Professor with the State Key Laboratory of Robotics and System, Harbin Institute of Technology. His current research interests include special robot systems, and aerospace mechanisms and control. He was elected as an Academician of the Chinese Academy of Engineering, in 2017.